

# Simultaneous light scattering and intrinsic fluorescence measurement for the classification of airborne particles

Paul H. Kaye, John E. Barton, Edwin Hirst, and James M. Clark

We describe a prototype laboratory light-scattering instrument that integrates two approaches to airborne particle characterization: spatial light-scattering analysis and intrinsic fluorescence measurement, with the aim of providing an effective means of classifying biological particles within an ambient aerosol. The system uses a single continuous-wave 266-nm ultraviolet laser to generate both the spatial elastic scatter data (from which an assessment of particle size and shape is made) and the particle intrinsic fluorescence data from particles in the approximate size range of 1–10- $\mu\text{m}$  diameter carried in a sample airflow through the laser beam. Preliminary results suggest that this multiparameter measurement approach can provide an effective means of classifying different particle types and can reduce occurrences of false-positive detection of biological aerosols. © 2000 Optical Society of America

OCIS codes: 120.5820, 120.1880, 290.5820, 290.1090, 300.2530.

## 1. Introduction

Driven by environmental, occupational, and defense concerns, there has been growing interest in methods that offer the potential of analyzing and characterizing airborne particles in real time. A particular objective has been to achieve differentiation between biological and nonbiological particles and (ideally) between various types of biological particles such that potential pathogens can be detected. Light-scattering-based instruments such as optical particle counters or aerodynamic particle sizers have long been a favored choice for airborne particle count and size monitoring as they offer close to real-time response and can operate continuously without the need for reagents, etc. For the discrimination of biological particles, particle intrinsic fluorescence offers significant potential, and several researchers have developed systems that incorporate particle fluorescence measurement in conjunction with the measurement of other particle parameters in an attempt to optimize discrimination.

In 1995, Pinnick *et al.*<sup>1</sup> described a laser-based particle counter that detected fluorescence and elastic scattering from individual airborne particles as they traversed the beam from a 488-nm argon-ion laser. The low levels of intrinsic fluorescence observed from kaolin, hematite, and polystyrene particles in comparison with that observed from several types of biological particles suggested that the instrument would be useful in discriminating biological from nonbiological particles. In an effort to enhance particle discrimination, the same researchers went on to extend the capabilities of the system to record the spectrum of fluorescence from a particle rather than simply the fluorescence magnitude.<sup>2,3</sup> More recently (1999) this research has been further developed by use of one of two UV excitation frequencies in place of the 488-nm beam. Results<sup>4</sup> showing the fluorescence spectra from individual 2–5- $\mu\text{m}$  biological aerosol particles excited by either 266- or 351-nm radiation from a Q-switched laser (Nd:YAG and Nd:YLF, respectively) illustrate the differences in fluorescence spectra that can be observed from different biological particles.

In 1997, Hairston *et al.*<sup>5</sup> described an instrument for the real-time detection of bioaerosols that incorporated simultaneous measurement of particle aerodynamic size and intrinsic fluorescence. The measurement of aerodynamic size in conjunction with fluorescence allows the generation of informative three-dimensional plots of particle size versus fluorescence versus count frequency. This system originally used 325-nm radiation from a helium–

---

P. H. Kaye (p.h.kaye@herts.ac.uk), J. E. Barton, and E. Hirst are with the Science and Technology Research Centre, University of Hertfordshire, Hatfield, Hertfordshire AL10 9AB, UK. J. M. Clark is with the Defence Evaluation and Research Agency, Chemical and Biological Defence, Porton Down, Salisbury, Wiltshire SP4 0JQ, UK.

Received 22 November 1999; revised manuscript received 4 April 2000.

0003-6935/00/213738-08\$15.00/0

© 2000 Optical Society of America

cadmium laser, but again this has since been modified for use with shorter UV radiation so as to achieve the excitation of additional biological fluorophores.

Seaver *et al.*<sup>6</sup> has recently developed an instrument that similarly records simultaneously an estimate of particle size (in this case based on elastic scatter) together with intrinsic particle fluorescence. Again, the ability to produce plots of fluorescent intensity against a scattered light signal has illustrated the potential of such dual-parameter measurements in the achievement of particle type discrimination.

Any monitoring system must aim for a minimum level of false positives. In the case of biological aerosols in a military situation, such events can lead to considerable effort being expended in taking protective measures and, if too frequent, will result in the monitor being mistrusted or, at worst, disregarded completely. In an attempt to further reduce the occurrence of false positives, such as may occur when nonbiological particles are present with similar size and fluorescence signature to biological particles, additional characteristics must be determined from the scattering particle. One method of achieving this is to examine the spatial pattern of light scattered elastically from the particle, from which both particle size and shape information can be deduced.

## 2. Spatial Light Scattering

The manner in which a particle spatially scatters incident light is a complex function of the size, shape, structure, and orientation of the particle, as well as of the properties of the illuminating radiation (wavelength, polarization state). With suitable control of some of these variables it is possible to determine parameters relating to the shape and structure of the scatterer. This spatial light-scattering analysis, also in certain geometries referred to as two-dimensional angular optical scattering,<sup>7</sup> has therefore been attracting considerable attention for particle characterization. Dick *et al.*<sup>8</sup> (1998) have used multiangle azimuthal measurements to determine the spherical and nonspherical fractions of laboratory and atmospheric aerosols; Holler *et al.*<sup>7</sup> (1998) used two-dimensional angular optical scattering to examine clusters of *Bacillus subtilis* var *niger* (BG) spores and found that island structures were observable in the spatial scattering patterns and that the number of these islands increased per unit solid angle with an increase in cluster diameter; Sachweh *et al.*<sup>9</sup> (1999) investigated spatial light scattering using three detection geometries and found that not only was good particle shape characterization obtainable, but also that, for supermicrometer particles, the surface structure of the particle contributed to the scattering pattern provided that the size of surface features substantially exceeded the wavelength of illumination.

We have also explored the potential of spatial light-scattering analysis<sup>10–12</sup> for particle shape characterization, and our research has resulted in a number of real-time monitoring systems for application in, for example, environmental aerosol monitoring<sup>13</sup> and as-

bestos fiber detection.<sup>14</sup> The prototype instrument described in this paper seeks to combine the advantages that spatial light-scattering analysis offers in terms of particle shape classification with those, demonstrated by the researchers referred to above, offered by intrinsic fluorescence.

## 3. Instrumentation

The prototype multiparameter scattering instrument is shown schematically in Fig. 1. The instrument employs a continuous-wave (cw) 266-nm laser (Coherent Verdi Nd:vanadate 532 nm with an external doubler to 266 nm; Coherent Inc., Santa Clara, Calif.). This laser, delivering up to 200 mW of output power in the UV, is used to produce both the spatial elastic scatter data from the particle (from which size and shape parameters are derived) and the necessary particle fluorescence excitation.

In operation, particle-laden air from a test aerosol is drawn through a scattering chamber at a rate of approximately 1 l/min. A filtered flow of sheath air aerodynamically focuses the sample airstream and constrains it to pass through the circularly polarized 266-nm beam from the UV laser. The airflow also has the effect of preferentially aligning elongated particles with their long axis parallel to the flow. This is an important attribute in the classification particle shape from the variation in azimuthal scattering.<sup>13,14</sup> At the point of intersection with the sample airflow, the beam dimensions are ~2 mm wide by ~100  $\mu\text{m}$  deep, ensuring that for particle number concentrations up to  $\sim 10^5/\text{l}$ , particle coincidences in the beam are rare. Light scattered both elastically and inelastically by the particle between the angles of 30°–140° to the beam axis is reflected from an ellipsoidal mirror and onto a photomultiplier tube (PMT) detector through a long-pass optical filter (295 nm, WG-295, CVI Laser Corp., Albuquerque, N.M.). The filter thus allows only the particle fluorescence signal to reach the detector.

Light scattered by the particle in the forward direction (between angles of 4° and 30°) is imaged onto a multipixel high-gain hybrid photodiode detector (HPD) (Delft Electronic Products BV, The Netherlands). It is this spatial scattering information that provides the particle shape classification. HPD's are similar to first-generation image intensifiers, employing a photocathode to convert optical to electron flux and accelerating the electrons (typically through ~10 kV) into a multipixel silicon diode structure where multiple electron-hole pairs are produced. Gains up to ~2000 are achievable within a compact, robust, and low-power package. The HPD used in our instrument has a custom-designed arrangement of 31 pixels in a 15-mm-diameter ring-wedge configuration as shown in Fig. 2. It comprises three concentric rings together with a center aluminized beam stop (shaded). The innermost ring, labeled 2, is continuous and provides the opportunity for particle detection regardless of particle orientation. The next two rings are divided into 6 and 24 segments, respec-

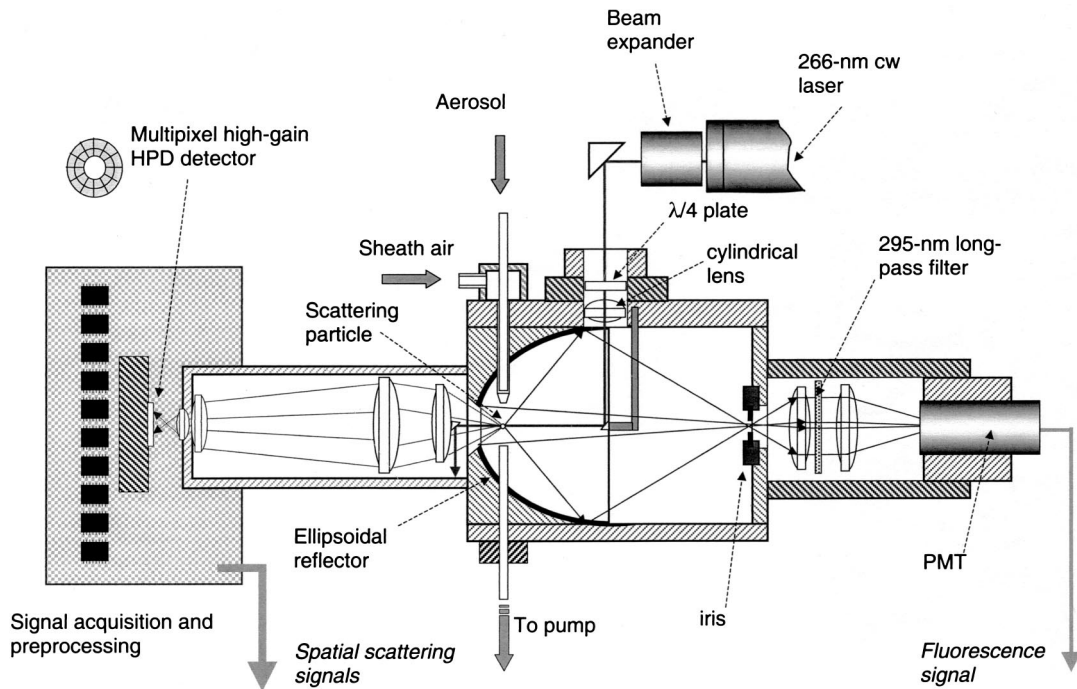


Fig. 1. Schematic diagram of the scattering chamber for the multiparameter scattering fluorescence instrument. The overall length of the chamber is 35 cm.

tively, to allow azimuthal and radial measurements of scattered light intensity.

The data-acquisition electronics are situated close to the HPD to minimize electrical noise interference. The electronics comprise 32 processing channels, 31 of which process data from the HPD and the 32nd processes data from the fluorescence PMT detector at the opposite end of the chamber. Each channel comprises a transimpedance amplifier, dc restoration circuitry (which removes any dc levels from the signals caused by background chamber illumination, etc), fol-

lowed by signal integration and digitization. The inner ring of the HPD acts also as a particle detect trigger, its output being passed to a comparator to initiate the particle detect sequence. Once the output level of this channel is above a user-defined threshold, the control logic forces the integrators for all 32 channels to commence integration. Integration terminates once the signal level on the trigger channel falls below the threshold. The integration period is typically 2  $\mu$ s, corresponding to the time of flight of a particle through the beam. The integrators hold their respective signal levels until they are passed to one of four 12-bit analog-to-digital converters, one for every eight channels. The subsequent digitized scattering and fluorescence values are multiplexed by way of serial data lines to the host computer for buffering and storage. Data can be acquired for particle throughput rates of up to  $\sim$ 5000 particles/s.

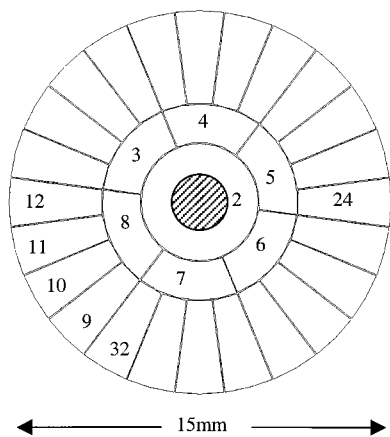


Fig. 2. Layout of the 31-pixel detector geometry used in the HPD spatial scattering detector. At the center is an aluminized beam stop. The output of the innermost annulus (2) is used as a particle detect trigger, and the segmented outer rings provide azimuthal scattering data from which an assessment of particle shape is made.

#### A. Data Display

Although spatial scattering and fluorescence data are stored in real time for subsequent analysis, the prototype instrument allows a simple real-time graphical display of the incoming data for diagnostic purposes. Figure 3 shows the screen display for a fiber particle (gypsum). The example also illustrates the effect that the inlet nozzle has on preferentially aligning elongated particles with their long axis parallel to the airflow. In the case of fiber particles, this results in essentially horizontal scattering (refer to Fig. 1), giving peak outputs at detector pixels 12 and 24 on the outer pixel ring, as shown in Fig. 3.

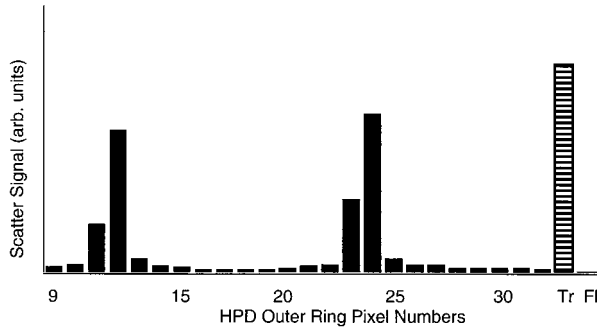


Fig. 3. Example display screen showing the output of the 24 outer-ring detector pixels resulting from a single gypsum fiber passing through the scattering volume. The vertical orientation of the fiber produces horizontal scattering as indicated by the high values in pixels 12 and 24. Tr, output of the trigger detect pixel 2; Fl, output of the fluorescence PMT detector.

Tr is the output of the trigger detect pixel 2, and Fl is the output of the fluorescence PMT detector.

#### B. Detector Gain Correction and Calibration

Before further processing, the data must be corrected for channel gain variations that arise in part from photocathode efficiency variation across the input window of the HPD. This is achieved by one's collecting data from known spherical particles such as polystyrene latex and normalizing the channel responses to these particles (on the grounds that known spherical particles should ideally produce an equal response in all detectors within a specified annulus). The data presented in this paper were corrected in this way.

### 4. Particle Classification

#### A. Scatter Intensity Versus Asymmetry Factor Plots

A convenient method of processing spatial light-scattering data to yield particle shape classification indices is through use of scatter intensity versus asymmetry factor (AF) plots.<sup>13</sup> The scatter intensity here is taken as the mean around the whole 360° of an azimuthal ring of detectors, and this yields a non-linear function related to the scattering cross section of the particle which can itself be correlated with a spherical-equivalent particle diameter by Mie theory.<sup>15</sup> The Af is a measure of the variation of the scattered light intensity around the azimuthal ring. It can be calculated with data from either the 6-pixel middle ring or the 24-pixel outer ring on the Delft Electronic Products HPD. The expression for calculation of Af is

$$Af = k \left[ \sum_{i=1}^n (\bar{E} - E_i)^2 \right]^{1/2} / \bar{E}, \quad (1)$$

where  $n$  is the number of pixels in the ring,  $E$  is the output value of each pixel,  $\bar{E}$  is the mean of all  $E$  values, and  $k$  is a constant to render the maximum possible value of Af to be 100. This maximum Af will occur when all but one pixel in an azimuthal ring are

zero. By applying this condition to Eq. (1), we can show  $k$  to be

$$k = 100 / \sqrt{n(n-1)}. \quad (2)$$

Clearly, in an ideal situation (with no experimental uncertainties), spherical particles that generated equal signals at each detector in the azimuthal ring will produce an Af = 0.

#### B. Scattering Asymmetry Performance Limits

As described above, the instrument uses the azimuthal variation of scattered light intensity to determine a particle shape (or asphericity) index Af. It was necessary, therefore, to determine first the instrumental limits of minimum-detectable azimuthal asymmetry and the linearity of the detector pixel responses throughout their usable dynamic range. The detection limits are set by the signal-to-noise ratio in the detector and by bandwidth and analog-to-digital conversion limitations within the signal acquisition and processing electronics. To determine this information, we used a pulsed light-emitting diode (LED) (~540 nm) to simulate particle transits through the laser beam by uniformly illuminating the whole of the HPD. The output of the LED was adjusted from zero to the maximum signal, which could be accommodated by the processing electronics, and this simulated particle data recorded and processed to yield a scatter intensity versus Af plot as described above.

Figure 4(a) shows the scatter intensity versus Af plot for the simulated particle data. As would be expected for uniform illumination of azimuthal pixels (simulating scattering by a perfect sphere<sup>15</sup>), the calculated Af values are close to zero throughout the majority of the LED output intensity range. However, at low intensities the calculated Af values increase markedly. This is more apparent in Fig. 4(b) that shows the same data plotted on a logarithmic ordinate and abscissa. Here the value of calculated Af increases almost linearly with decreasing input signal magnitude. This is principally attributable to shot noise in the detected analog signals from the detector pixels, causing significant variation in the digitized signal values that in turn result in increased Af values. The solid curve in Fig. 4(b) indicates the approximate limit of performance of the system in terms of particle shape characterization: Perfectly spherical scatterers would produce data points along this curve; Af values to the right of the curve can be interpreted as azimuthal variations in scattering arising predominantly from nonspherical particle shape or structure.

### 5. Preliminary Experimental Results

#### A. Spatial Scattering Data

The HPD was of a new and untried design, the first objective was to evaluate the spatial scattering data it recorded and assess the potential of these data for particle classification. For ease of optical alignment,

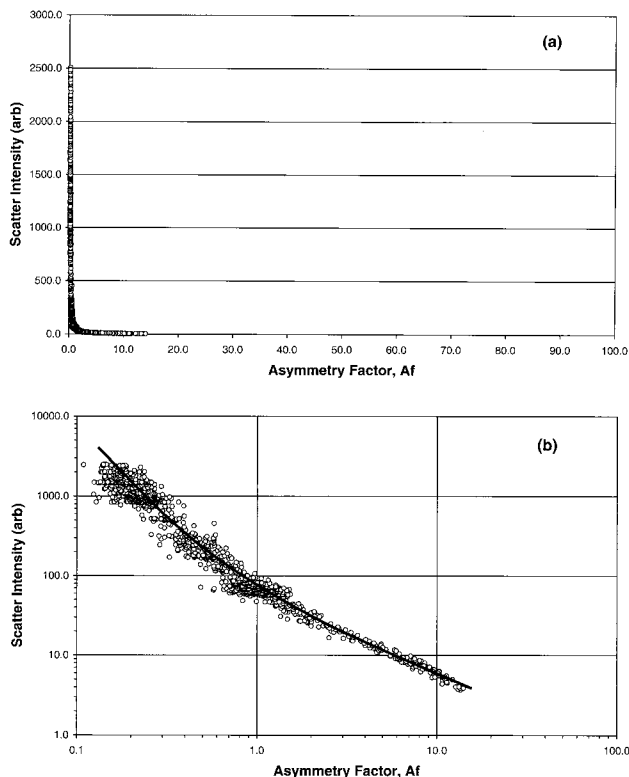


Fig. 4. (a) Scatter intensity versus Af plot for simulated spherical particle data (produced by uniform illumination of the HPD from a pulsed LED source). Ideally such data should lie entirely along the ordinate ( $Af = 0$ ) corresponding to perfectly spherical scatterers. (b) As in (a) but with logarithmic scales. The solid curve represents the noise-limited performance of the system in terms of particle shape characterization: Perfectly spherical scatterers would produce data points along this curve, and nonspherical scatterers would result in data points to the right of the curve.

this initial assessment of the HPD was carried out with an illumination wavelength of 532 nm rather than 266 nm. This also allowed unwanted sources of background scattering within the scattering chamber to be identified and minimized before the implementation of the shorter wavelength. Use of 532-nm illumination precluded the measurement of particle fluorescence at this stage.

Figure 5 shows scatter intensity versus Af plots for a variety of aerosol types: water droplets, hematite grains, BG spores, and gypsum dust. The hematite is prolate ellipsoidal in shape with a major axis  $\sim 2\text{--}3\ \mu\text{m}$  and with an aspect ratio typically 3:1. It is similar in size and shape to the BG spores. The gypsum has an irregular fibrous morphology, with aspect ratios from  $\sim 3:1$  to  $8:1$  and lengths up to  $\sim 10\ \mu\text{m}$ . Each aerosol was generated independently. We aerolized the dry-powder hematite and gypsum using a compressed air jet into a ballast chamber from which the instrument sample flow was drawn. The BG spores were aerolized into the ballast chamber with a nebulizer. The water droplets were sprayed directly over the vicinity of the instrument inlet. The spray was independently measured with an Aerodynamic Particle Sizer (APS model 3320, TSI

Inc., St. Paul, Minn.) which indicated that the droplets were polydisperse with a distribution of aerodynamic diameters from  $\sim 1\ \mu\text{m}$  to greater than  $10\ \mu\text{m}$ , although the largest of these droplets lay outside the measurable size range of our prototype instrument.

Features to note from Fig. 5 are

(a) As would be expected, scattering data for the droplets lie close to the instrument performance limit for spherical particles with Af values generally less than unity. The droplets were clearly distinguishable from the nonspherical hematite and gypsum particles which exhibit Af values from  $\sim 5$  to  $\sim 60$ .

(b) The results suggest that the aerosolization process did not completely break down the dry hematite into the fundamental particles. Agglomerates up to the top of the measurable range ( $\sim 10\ \mu\text{m}$ ) were recorded. The lower Af values of these agglomerates indicate that they assumed a more spherical shape than the individual ellipsoidal grains.

(c) There is significant overlap between the hematite, gypsum (at their lower size range), and BG spore data. This might be expected as the morphologies of the hematite and lower aspect ratio gypsum particles are somewhat similar to that of the spores. It is this type of particle classification ambiguity that the additional parameter of particle fluorescence is intended to mitigate.

#### B. Spatial Scattering and Fluorescence Measurements

We acquired preliminary data using the 266-nm radiation for simultaneous spatial scattering and fluorescence excitation. The spatial scattering data obtained at this wavelength were used to produce the scatter intensity versus Af plot shown in Fig. 6. Data are presented for  $1\text{-}\mu\text{m}$ - and  $3\text{-}\mu\text{m}$ -diameter polystyrene latex (PSL) spheres (Dow Corning),  $1.7\text{-}\mu\text{m}$ -diameter fluorescent PSL spheres (Polyscience Inc. Fluoresbright), gypsum, and BG spores. Unfortunately, hematite samples were not available at the time of these tests.

Figure 6 shows all three varieties of PSL spheres close to the instrument performance limit for spherical particles, although the range of Af values was comparatively large for the  $1\text{-}\mu\text{m}$  PSL. It is suspected that this was a result of significant occurrences of doublets and higher-order multiplets being present in the aerosol from the nebulizer. The BG spore data and gypsum data once again show a substantial overlap in the  $10\text{--}30$  Af range, making differentiation of these particles impossible from the scatter intensity and Af data alone. The spread of scatter intensity levels for all three varieties of PSL is larger than would be expected given the inherent size uniformity of these materials. The principal reason for the spread is the variation in beam intensity across the scattering volume (i.e., the intersection between the beam and the sample airflow). Although the airflow column diameter is less than the beam width, the Gaussian profile of the beam makes completely uniform illumination of the scattering volume impossible.

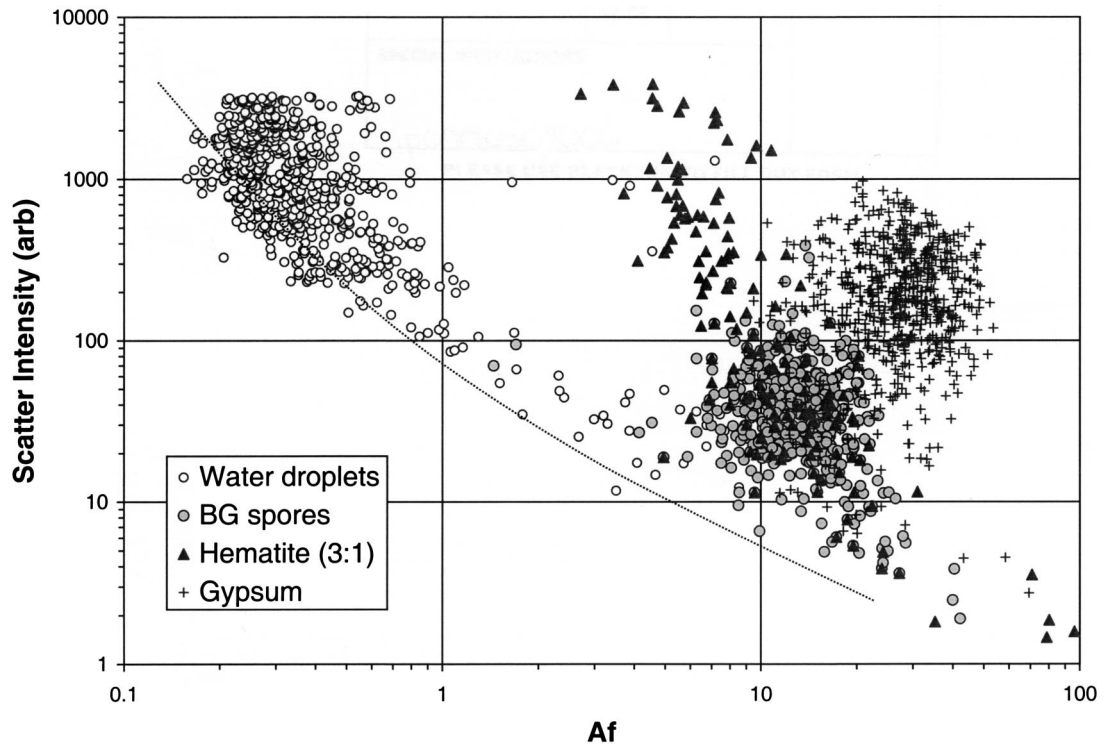


Fig. 5. Scatter intensity versus Af plots recorded at a 532-nm wavelength for aerosols of water droplets, hematite grains, BG spores, and gypsum dust. The dotted curve again represents the limit of performance for perfectly spherical scatterers.

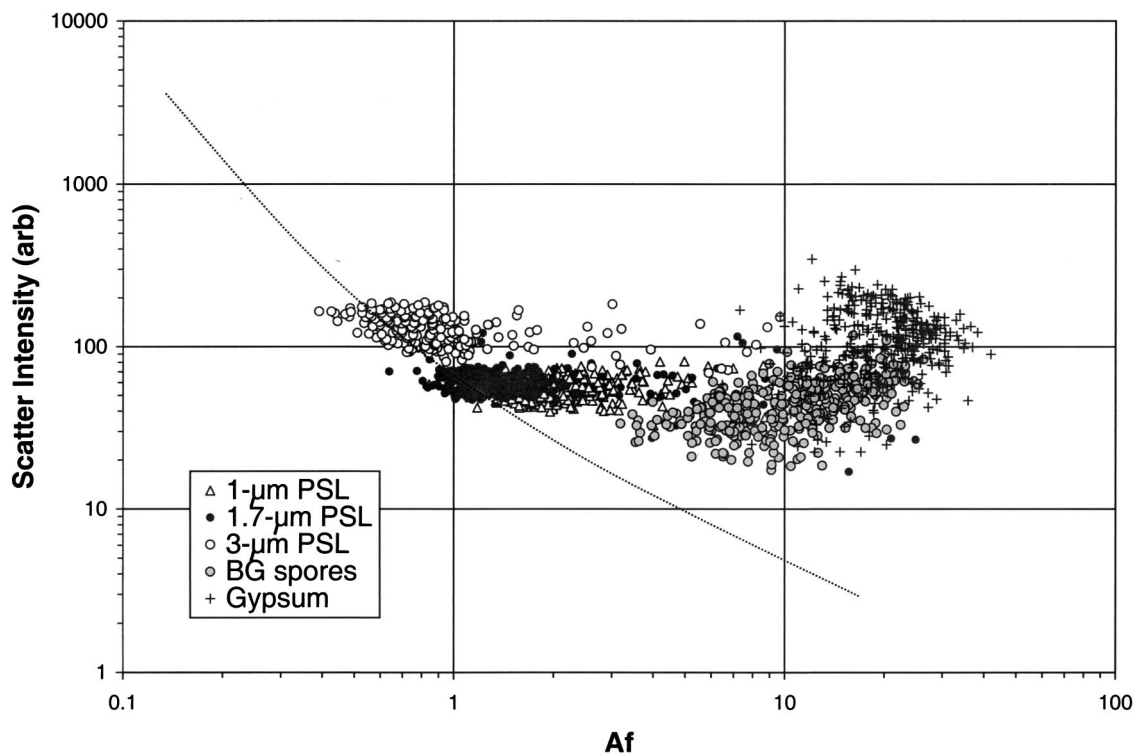


Fig. 6. Scatter intensity versus Af plots recorded at a 266-nm wavelength for aerosols of 1- $\mu$ m PSL, 3- $\mu$ m PSL, 1.7- $\mu$ m fluorescent PSL, BG spores, and gypsum dust. The dotted curve again represents the limit of performance for perfectly spherical scatterers.

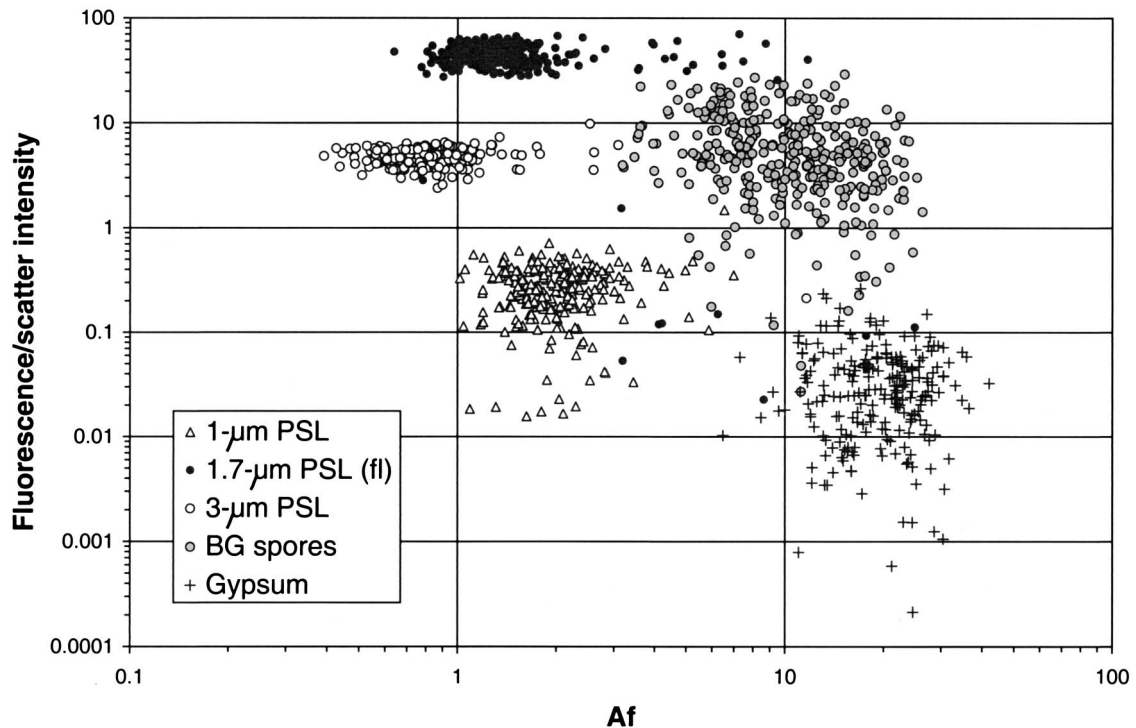


Fig. 7. Graph of fluorescence amplitude and scatter intensity versus Af for the same aerosol data as shown in Fig. 6.

Figure 7 shows the same particle data as Fig. 6, but in this case the degree of intrinsic particle fluorescence has been introduced in addition to scatter intensity and Af. The graph shows the ratio of particle fluorescence divided by scatter intensity as a function of particle Af. This is a simplistic approach to normalizing the fluorescence signal for particle volume but nevertheless it provides an effective means of data separation. As can be seen from Fig. 7, the fluorescent 1.7- $\mu\text{m}$  PSL is, as would be expected, clearly differentiated from the nonfluorescent PSL varieties, having an order of magnitude greater fluorescence to scatter intensity ratio. The outlying data points for the fluorescent PSL (up to values of Af = 10) occur at virtually constant fluorescence to scatter intensity ratios, again suggesting these are the product of doublets and multiplets in the aerosol.

More importantly, the BG spores and gypsum, indistinguishable on the scatter intensity versus Af plot, are widely separated in Fig. 7 as a result of the substantial differences in intrinsic fluorescence of the two materials.

## 6. Discussion

The instrument described in this paper is at an early stage of development but has nevertheless yielded encouraging results so far. The unique combination of particle shape and size characterization from spatial scattering analysis together with intrinsic fluorescence measurement offers a powerful method of classifying airborne particle types and, in particular, offers potentially enhanced discrimination between biological and nonbiological particles. We are currently in the process of refining the instrument to

improve the uniformity of scattering volume irradiance and further reduce background optical noise. This will be followed by an extensive program of experimental trials covering a wide variety of biological and nonbiological materials to fully assess the degree of particle discrimination that can be achieved in the field. Beyond this, there exists the possibility of our spectrally interrogating the fluorescence signatures of the particles under test. Other researchers<sup>3,4</sup> have shown that such spectra can provide additional characteristic information to enhance discrimination.

Use of a single cw UV laser to acquire both elastic scatter and fluorescence data offers some advantages over systems<sup>3-6</sup> that utilize a pulsed UV source triggered by a separate cw visible laser: First it simplifies the optomechanical arrangement of the light-scattering chamber and removes the need for the high-speed triggering circuitry that is required in the pulsed UV laser systems; second, the short UV wavelength (266 nm compared with 532–650 nm used in our previous shape classification instruments<sup>13,14</sup>) theoretically improves the sensitivity of the instrument to particle shape variations, especially for the smaller micrometer-sized range into which many airborne bio-organisms fall; third, because the particle is exposed to UV power levels that are far lower than experienced in the pulsed laser fluorescence systems (200 mW for  $\sim 2 \mu\text{s}$  compared with tens of watts for nanoseconds), the potential problems of photobleaching of the fluorescent molecules within the particle which can occur at high irradiances are lessened. However, against these advantages, the cw laser system we are using is large and delicate and impractical for use in a field instru-

ment. Such field implementation will require the development of more compact and robust cw UV laser sources.

This research has been supported by grants from the UK Defence Evaluation Research Agency, Porton Down.

## References

1. R. G. Pinnick, S. C. Hill, P. Nachman, J. D. Pendleton, G. L. Fernandez, M. W. Mayo, and J. G. Bruno, "Fluorescence particle counter for detecting airborne bacteria and other biological particles," *Aerosol Sci. Technol.* **23**, 653–664 (1995).
2. P. Nachman, G. Chen, R. G. Pinnick, S. C. Hill, R. K. Chang, M. W. Mayo, and G. L. Fernandez, "Condition sampling spectrograph detection system for fluorescent measurements of individual airborne biological particles," *Appl. Opt.* **35**, 1069–1076 (1996).
3. G. Chen, P. Nachman, R. G. Pinnick, S. C. Hill, and R. K. Chang, "Conditional-firing aerosol-fluorescence spectrum analyzer for individual airborne particles with pulsed 266-nm laser excitation," *Opt. Lett.* **21**, 1307–1309 (1996).
4. Y. Pan, S. Holler, R. K. Chang, S. C. Hill, R. G. Pinnick, S. Niles, and J. R. Bottiger, "Single-shot fluorescence spectra of individual micrometer-sized bioaerosols illuminated by a 351- or 266-nm ultraviolet laser," *Opt. Lett.* **24**, 116–118 (1999).
5. P. P. Hairston, J. Ho, and F. R. Quant, "Design of an instrument for real-time detection of bioaerosols using simultaneous measurement of particle aerodynamic size and intrinsic fluorescence," *J. Aerosol Sci.* **28**, 471–482 (1997).
6. M. Seaver, J. D. Eversole, J. J. Hardgrove, W. K. Cary, Jr., and D. C. Roselle, "Size and fluorescence measurements for field detection of biological aerosols," *Aerosol Sci. Technol.* **30**, 174–185 (1999).
7. S. Holler, Y. Pan, R. K. Chang, J. R. Bottiger, S. C. Hill, and D. B. Hillis, "Two-dimensional angular optical scattering for the characterization of airborne microparticles," *Opt. Lett.* **23**, 1489–1491 (1998).
8. W. D. Dick, P. J. Ziemann, P.-F. Huang, and P. H. McMurray, "Optical shape fraction measurements of submicrometre laboratory and atmospheric aerosols," *Meas. Sci. Technol.* **9**, 183–196 (1998).
9. B. Sachweh, H. Barthel, R. Polke, H. Umhauer, and H. Buttner, "Particle shape and structure analysis from the spatial intensity pattern of scattered light using different measuring devices," *J. Aerosol Sci.* **30**, 1257–1270 (1999).
10. E. Hirst, P. H. Kaye, and J. R. Guppy, "Light scattering from nonspherical airborne particles: experimental and theoretical comparisons," *Appl. Opt.* **33**, 7180–7186 (1994).
11. E. Hirst and P. H. Kaye, "Experimental and theoretical light scattering profiles from spherical and non-spherical particles," *J. Geophys. Res. D* **101**, 19,231–19,235 (1996).
12. P. H. Kaye, "Spatial light scattering as a means of characterising and classifying non-spherical particles," *Meas. Sci. Technol.* **9**, 141–149 (1998).
13. P. H. Kaye, K. Alexander-Buckley, E. Hirst, and S. Saunders, "A real-time monitoring system for airborne particle shape and size analysis," *J. Geophys. Res. D* **101**, 19,215–19,221 (1996).
14. E. Hirst, P. H. Kaye, and Z. Wang-Thomas, "Neural-network-based spatial light-scattering instrument for hazardous airborne fiber detection," *Appl. Opt.* **36**, 6149–6156 (1997).
15. C. F. Bohren and D. R. Huffman, *Absorption and Scattering of Light by Small Particles* (Wiley, New York, 1983).